A Systematic and Numerical Methodology for GaN HEMT Current-Gain Peak Analysis Using the Complex Lorentzian Function

Giovanni Gugliandolo, *Member, IEEE*, Giovanni Crupi, *Senior Member, IEEE*, Valeria Vadalà, *Member, IEEE*, Antonio Raffo, *Member, IEEE*, Nicola Donato, *Senior Member, IEEE*, and Giorgio Vannini, *Member, IEEE*

***Abstract*— The purpose of this letter is to present a measurement-based analysis of the transistor current-gain peak (CGP), which consists of a sudden peak in the magnitude of the short-circuit current-gain (h_{21}) at a certain frequency. A systematic and numerical approach is proposed to analyze CGP. This powerful and technology-independent methodology is based on developing an accurate fitting of the experiments using the complex Lorentzian function, thus allowing an accurate and straightforward extraction of the parameters describing CGP. The validity of the developed technique is fully demonstrated by its application to the analysis of CGP for a gallium nitride (GaN) high-electron-mobility transistor (HEMT) at different ambient temperatures and bias conditions.**

***Index Terms*— Current-gain peak (CGP), fitting, gallium nitride (GaN), high-electron-mobility transistor (HEMT), parameter extraction, scattering parameter measurements.**

I. Introduction

To meet the increasing demand requirements of high-frequency and ultra-wideband applications, transistor technologies are aggressively pushed to perform faster. A well-known figure-of-merit to quickly assess the high-frequency performance of a transistor is the unity current-gain cut-off frequency (f_T), which is given by the frequency where the short-circuit current-gain (h_{21}) becomes unity. Though much of the interest in achieving an active transistor operation even at frequencies beyond f_T has been directed toward bipolar transistors [1], [2], [3], [4], [5], [6], [7], [8], such as the so-called resonance phase transistor (RPT) [1], [2], [3], [4], [5], [6], recent efforts have been made to study the current-gain peak (CGP) for field-effect transistors (FETs) [9], [10], [11], [12], [13], [14], [15], [16], [17]. CGP consists of a peak easily detectable by plotting the magnitude of h_{21} in decibels versus frequency on a log scale. CGP has been studied in terms of equivalent-circuit elements, and its appearance has been attributed to the resonance between the extrinsic inductances (i.e., the sum of L_d and L_s) and the intrinsic capacitances (i.e., the parallel connection of C_{ds} and the series connection of C_{gs} and C_{gd}) [9]. CGP has been studied also in terms of poles and zeros, and a simplified mathematical expression has been proposed to calculate the location of the peak [14]. As CGP consists of an abrupt change in the magnitude of h_{21} at a certain frequency, this anomalous peak can be seen as a kink effect affecting h_{21}. Hence, analogously to what has been done for the kink effect in the output reflection coefficient (S_{22}) [18], CGP can be investigated in terms of the second derivative (D2) of the magnitude of h_{21} in decibels versus frequency, enabling the determination of a set of parameters to fully and systematically characterize this kink effect. Due to the high sensitivity to noise of the second derivative, trustworthy values of the kink parameters cannot be calculated directly from measurements. Therefore, model simulations [e.g., equivalent circuits and artificial neural networks (ANNs)] or fitting functions are required to obtain a smooth behavior of D2. To reduce the modeling effort and to enable a more accurate reproduction of the experiments, scattering (S-) parameters have been straightforwardly modeled using ANNs [19] and then, CGP has been described with a set of kink parameters [11]. Recently, an alternative approach has been proposed to quantify CGP by measuring the area of CGP (ACGP) as the zone between the two curves corresponding to h_{21} with and without the peak [15]. This task has been done by using a commercial plot digitizer without the need of determining a model able to approximate the measurements.

Here, we propose a novel methodology based on developing a fitting procedure using a complex Lorentzian function [20] to reproduce the frequency-dependent behavior of h_{21}, thereby allowing an accurate determination of a set of kink parameters describing CGP systematically and numerically. The developed methodology is applied to the gallium nitride (GaN) technology, as its operating frequency keeps extending

Manuscript received 10 January 2023; revised 8 March 2023; accepted 2 April 2023. Date of publication 1 May 2023; date of current version 7 July 2023. This work was supported in part by the Italian Ministry of University and Research (MUR) through the PRIN 2017 Project under Grant 2017FL8C9N. *(Corresponding author: Giovanni Crupi.)*

Giovanni Gugliandolo and Nicola Donato are with the Engineering Department, University of Messina, 98166 Messina, Italy (e-mail: giovanni.gugliandolo@unime.it; nicola.donato@unime.it).

Giovanni Crupi is with the BIOMORF Department, University of Messina, 98125 Messina, Italy (e-mail: crupig@unime.it).

Valeria Vadalà is with the Department of Physics, University of Milano-Bicocca, 20126 Milano, Italy (e-mail: valeria.vadala@unimib.it).

Antonio Raffo and Giorgio Vannini are with the Department of Engineering, University of Ferrara, 44122 Ferrara, Italy (e-mail: antonio.raffo@unife.it; giorgio.vannini@unife.it).

Color versions of one or more figures in this letter are available at https://doi.org/10.1109/LMWT.2023.3264904.

Digital Object Identifier 10.1109/LMWT.2023.3264904

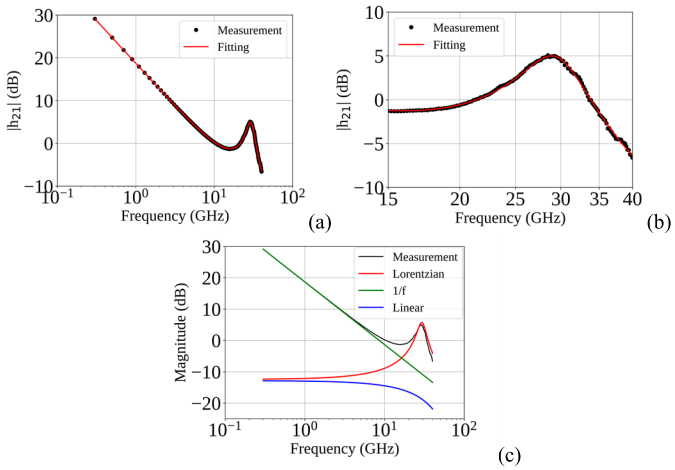

Fig. 1. Measured (dots) and fitted (line) h_{21} for a GaN HEMT at $V_{GS} = -2$ V, $V_{DS} = 19$ V, and $T_a = 80$ °C with two frequency ranges from (a) 0.3 to 40 and (b) 15 to 40 GHz. (c) Illustration of the magnitude in decibels of the three terms of the complex function used to fit the measured h_{21} [(see (1)].

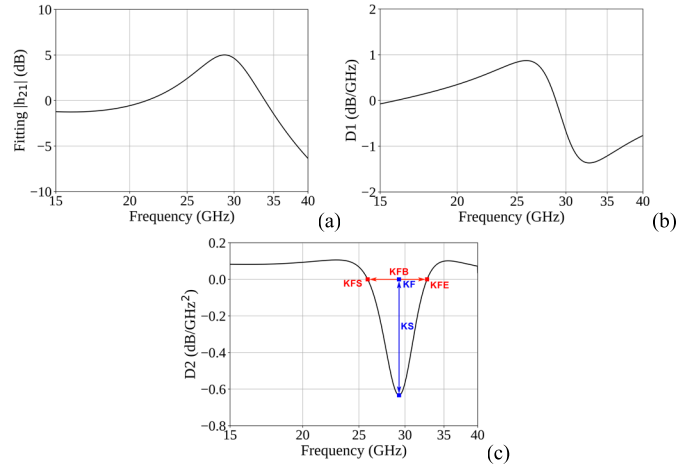

Fig. 2. (a) Fit h_{21} from 15 to 40 GHz and its (b) first and (c) second derivatives with the illustration of extraction of the kink parameters KFS, KFE, KFB, KF, and KS for a GaN HEMT at $V_{GS} = -2$ V, $V_{DS} = 19$ V, and $T_a = 80$ °C.

further in the mm-wave range [21], [22], [23], [24], [25]. The described procedure is technology independent, so, as a criterion of choice, we selected a device for which a complete measurement set was available. In particular, the studied device is a aluminium gallium nitride (AlGaN)/GaN high-electron-mobility transistor (HEMT) on SiC substrate with a gate length of 0.7 μm and a gate width of 2 × 400 μm. Experiments consist of multibias S-parameters measured from 300 MHz to 40 GHz with a frequency step of 198.5 MHz at five ambient temperatures (T_a): 20 °C, 35 °C, 50 °C, 65 °C, and 80 °C. The proposed methodology is used to fit h_{21} versus frequency without the need of modeling all the four S-parameters and, subsequently, to determine the parameters describing CGP, thereby enabling the analysis of the effects of varying bias and temperature conditions.

II. Fitting Procedure

The behavior of h_{21} as a function of the frequency (f) has been modeled by using the following complex function:

$$h_{21}(f) = \frac{Q/S}{1 + 2jQ\left(\frac{f - f_r}{f_r}\right)} + \frac{a}{f} + bf + c. \quad (1)$$

The first term is a complex Lorentzian function used to describe the resonant peak occurring in the high-frequency range [20], [26], [27]. f_r is its resonant frequency, Q is the quality factor of the peak, S is a complex coefficient, and i is the imaginary unit. The second term (i.e., a/f), where a is a complex coefficient, is used to model the response of h_{21} at lower frequencies. Moreover, a complex linear function (i.e., $bf + c$) has been included to reduce the fitting residuals by modeling the background effects over the considered frequency range [28], [29], [30]. The fitting procedure has been implemented in Python using the lmfit library, and the optimized coefficients have been calculated by means of the Levenberg–Marquardt algorithm. A comparison between the measured and fitted h_{21} for the whole studied frequency range is reported in Fig. 1(a). The coefficient of determination (i.e., R^2) has been estimated for each fitting. It is a goodness-of-fit statistic that describes how well the model explains the measurements carried out [31]. In this study, the R^2 is better than 0.99, indicating a strong correlation between the measured and fitted data. To better highlight the fitting performance in the region close to CGP, Fig. 1(b) shows the comparison for the limited frequency range from 15 to 40 GHz. Finally, to give an intuitive idea on how the three complex terms in (1) contribute to reproducing the behavior of h_{21}, Fig. 1(c) shows the magnitude in decibels of h_{21} together with the magnitude in decibels of the three terms.

In addition to Q-factor and f_r, which are straightforwardly estimated from the complex Lorentzian function, and to the kink amplitude (KA), which is the value of the fitted h_{21} at the resonance frequency, the kink parameters include the following ones evaluated from D2 (see Fig. 2).

1) The kink frequency band (KFB) is the frequency range going from the kink frequency start (KFS) to the kink frequency end (KFE), i.e., the frequencies of CGP onset and disappearance, which are defined as the two frequencies where D2 becomes 0.

2) The kink size (KS) represents the CGP size and is given by the negative peak value of D2 occurring at the kink frequency (KF).

3) The kink shape factor (KSF) is calculated as the ratio between KF and KFB.

III. Experimental Results

Figs. 3 and 4 highlight the impact of changing T_a and V_{DS} on CGP by showing both the frequency-dependent behavior of h_{21} and the kink parameters. Although f_r and KF are defined in different ways for determining the frequency occurrence of CGP (i.e., f_r can be estimated from the complex Lorentzian function while KF is obtained from D2 of the fitted h_{21}), Figs. 3(c) and 4(c) show that almost the same values of these two parameters are obtained, confirming their validity. Similarly, although the Q-factor and KSF are defined in different ways for representing the ratio between the frequency

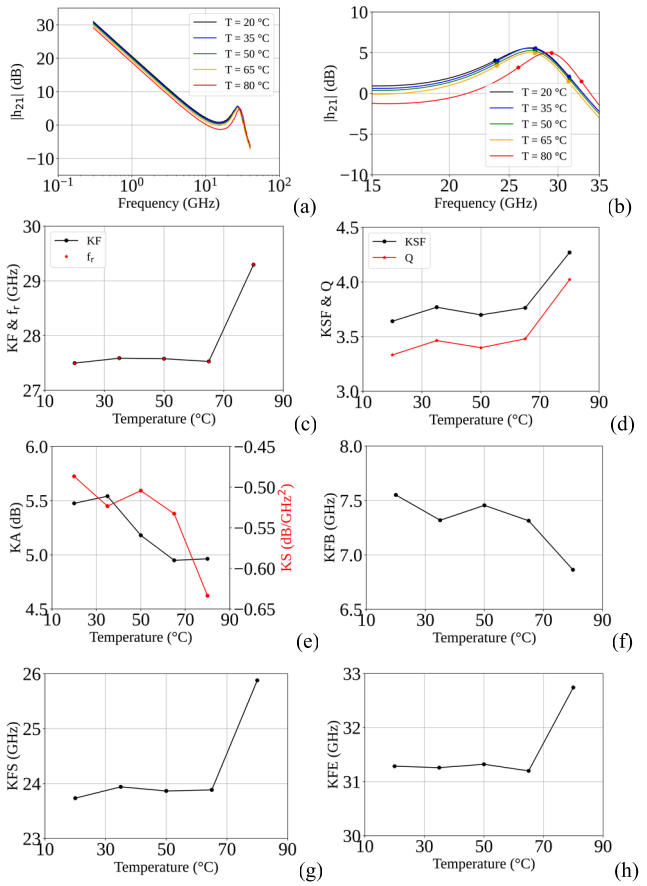

Fig. 3. (a) Measured h_{21} from 0.3 to 40 GHz for a GaN HEMT at $V_{GS} = -2$ V and $V_{DS} = 19$ V with five different values of T_a. (b) CGP is highlighted with three squares at the evaluated frequencies of the onset, peak, and disappearance of CGP in the fitted h_{21} from 15 to 35 GHz. (c)–(h) Parameters describing CGP versus T_a going from 20 °C to 80 °C with a step of 15 °C.

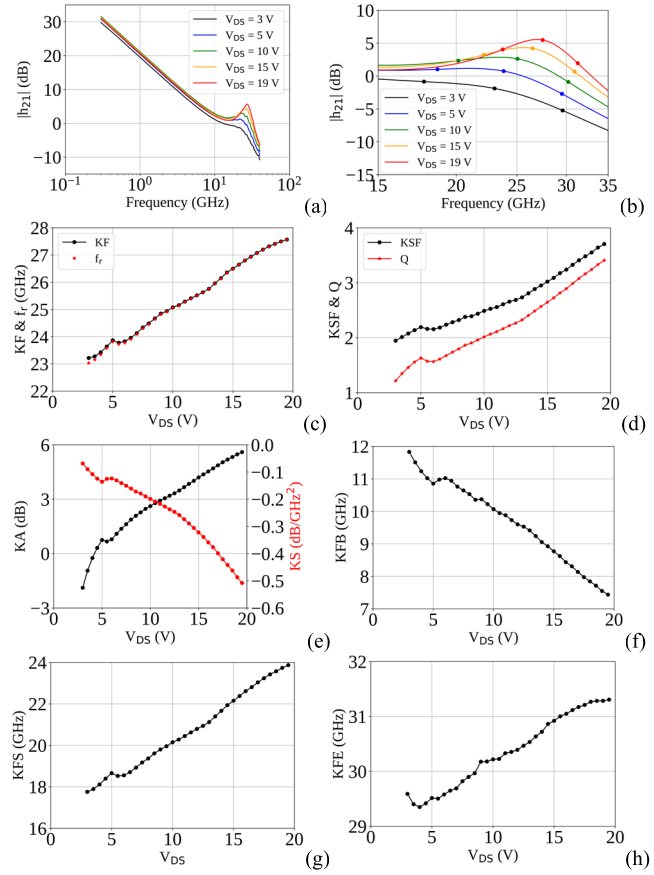

Fig. 4. (a) Measured h_{21} from 0.3 to 40 GHz for a GaN HEMT at $V_{GS} = -2$ V and $T_a = 20$ °C with five different values of V_{DS}. (b) CGP is highlighted with three squares at the evaluated frequencies of the onset, peak, and disappearance of CGP in the fitted h_{21} from 15 to 35 GHz. (c)–(h) Parameters describing CGP versus V_{DS} going from 3 to 19 V with a step of 0.5 V.

occurrence of CGP and its bandwidth (i.e., Q-factor is defined as the ratio of f_r to the 3-dB bandwidth and is estimated from the complex Lorentzian function, whereas the KSF is given by the ratio between KF and KFB that is calculated from D2 of the fitted h_{21}), Figs. 3(d) and 4(d) show a good agreement between these two parameters, confirming their validity.

As can be seen in Figs. 3(e) and 4(e), the parameters KA and the magnitude of KS, which are defined in different ways to quantify the size of CGP (i.e., KA and KS are estimated at the frequency occurrence of CGP from the fit h_{21} and from its D2, respectively), show similar trends but with some discrepancies (e.g., Fig. 3(e) shows that, by heating the device at 80 °C, KA is reduced while |KS| is increased), demonstrating the need of defining KS for evaluating the level of enhancement of CGP as higher values of h_{21} do not necessarily imply an enhanced CGP.

By heating the device, the most evident effect on h_{21} is the reduction of its low-frequency magnitude [see Fig. 3(a)], due to the degradation of the carrier transport properties and, then, of the intrinsic transconductance (g_m) [32]. KF shows only a weak dependence on T_a, consistent with the fact that the extrinsic inductances and the intrinsic capacitances depend only slightly on the temperature.

Fig. 4(b) shows that variations in V_{DS} have a very strong impact on CGP, which disappears at low V_{DS} values because of the increase in the intrinsic output conductance (g_{ds}) which tends to short circuit the contributions of the intrinsic capacitances [9]. By lowering V_{DS}, CGP becomes less pronounced (as can be quantified by the reduction in the magnitude of KS and in KA) and appears at low frequencies (as can be quantified by the reduction in KF, KFS, and KFE) and over a wider frequency range (as can be quantified by the broader KFB). In addition, the shift of CGP at low frequencies and over a broader frequency range leads to a reduction in both the Q-factor and KSF.

IV. Conclusion

A fitting procedure based on a complex Lorentzian function was developed and, then, successfully applied to mimic the frequency-dependent behavior of the transistor short-circuit current gain. The optimized coefficients were calculated using the Levenberg–Marquardt algorithm. The fit function was used for determining the parameters that allow one to fully characterize CGP systematically and numerically. Although a GaN HEMT at different T_a and bias conditions was considered as a case study, the proposed methodology is general and technology independent and, then, applicable for investigating CGP for any type of transistor with respect to different factors.

REFERENCES

[1] A. A. Grinberg and S. Luryi, "Coherent transistor," *IEEE Trans. Electron Devices*, vol. 40, no. 8, pp. 1512–1522, Aug. 1993.

[2] S. Luryi, J. Xu, and A. Zaslavsky, *Future Trends in Microelectronics: Reflections on the Road to Nanotechnology*. Dordrecht, The Netherlands: Kluwer, 1996.

[3] H. Jorke and M. Schafer, "Resonance phase operation of bipolar transistors," in *Proc. Top. Meeting Silicon Monolithic Integr. Circuits RF Syst.*, Garmisch, Germany, Apr. 2003, pp. 26–28.

[4] E. Kasper et al., "SiGe resonance phase transistor: Active transistor operation beyond the transit frequency f_T," *Solid-State Electron.*, vol. 48, no. 5, pp. 837–840, May 2004.

[5] S. Heim, R. Wanner, M. Stoffel, and E. Kasper, "Resonance phase operation of a SiGe HBT," *Mater. Sci. Semicond. Process.*, vol. 8, nos. 1–3, pp. 319–322, Feb. 2005.

[6] J. D. Cressler, *Silicon Heterostructure Devices*. Boca Raton, FL, USA: CRC Press, 2008.

[7] J.-S. Rieh et al., "Small- and large-signal operation of X-band CE and CB SiGe/Si power HBT's," in *IEEE MTT-S Int. Microw. Symp. Dig.*, Anaheim, CA, USA, Jun. 1999, pp. 1191–1194.

[8] Z. Ma, S. Mohammadi, P. Bhattacharya, L. P. B. Katehi, S. A. Alterovitz, and G. E. Ponchak, "Power performance of X-band Si/$Si_{0.75}Ge_{0.25}$/Si HBTs," in *Proc. Top. Meeting Silicon Monolithic Integr. Circuits RF Syst.*, Ann Arbor, MI, USA, Sep. 2001, pp. 170–176.

[9] G. Crupi, A. Raffo, D. M. P. Schreurs, G. Avolio, A. Caddemi, and G. Vannini, "A clear-cut understanding of the current-gain peak in HEMTs: Theory and experiments," *Microw. Opt. Technol. Lett.*, vol. 54, no. 12, pp. 2801–2806, Dec. 2012.

[10] G. Crupi et al., "Identification of the intrinsic capacitive core for GaAs HEMTs by investigating the frequency behavior of the impedance parameters," *Microw. Opt. Technol. Lett.*, vol. 55, no. 6, pp. 1237–1240, Jun. 2013.

[11] G. Crupi et al., "An extensive experimental analysis of the kink effects in S_{22} and h_{21} for a GaN HEMT," *IEEE Trans. Microw. Theory Techn.*, vol. 62, no. 3, pp. 513–520, Mar. 2014.

[12] G. Crupi et al., "Technology-independent analysis of the double current-gain peak in millimeter-wave FETs," *IEEE Microw. Wireless Compon. Lett.*, vol. 28, no. 4, pp. 326–328, Apr. 2018.

[13] G. Crupi, A. Raffo, V. Vadalà, G. Vannini, and A. Caddemi, "A new study on the temperature and bias dependence of the kink effects in S_{22} and h_{21} for the GaN HEMT technology," *Electronics*, vol. 7, no. 12, p. 353, Nov. 2018.

[14] S. A. Ahsan, S. Ghosh, S. Khandelwal, and Y. S. Chauhan, "Pole-zero approach to analyze and model the kink in gain-frequency plot of GaN HEMTs," *IEEE Microw. Wireless Comp. Lett.*, vol. 27, no. 3, pp. 266–268, Nov. 2017.

[15] M. A. Alim, M. A. Hasan, A. A. Rezazadeh, C. Gaquiere, and G. Crupi, "Multibias and temperature dependence of the current-gain peak in GaN HEMT," *Int. J. RF Microw. Comput.-Aided Eng.*, vol. 30, no. 4, Apr. 2020, Art. no. e22129.

[16] P. K. Kaushik, S. K. Singh, A. Gupta, and A. Basu, "Small-signal analysis of channel resistance R_L at low gate bias voltages in AlGaN/GaN HEMTs," *IEEE Trans. Electron Devices*, vol. 68, no. 12, pp. 6033–6038, Dec. 2021.

[17] P. K. Kaushik et al., "Simulation-based study of current gain peaks h_{21} at low gate bias in AlGaN/GaN HEMTs," *Eng. Res. Exp.*, vol. 4, no. 2, Jun. 2022, Art. no. 025042.

[18] G. Crupi, A. Raffo, A. Caddemi, and G. Vannini, "The kink phenomenon in the transistor S_{22}: A systematic and numerical approach," *IEEE Microw. Wireless Compon. Lett.*, vol. 22, no. 8, pp. 406–408, Aug. 2012.

[19] Z. Marinković et al., "Neural approach for temperature-dependent modeling of GaN HEMTs," *Int. J. Numer. Model., Electron. Netw., Devices Fields*, vol. 28, no. 4, pp. 359–370, Jul./Aug. 2015.

[20] M. S. Khalil, M. J. A. Stoutimore, F. C. Wellstood, and K. D. Osborn, "An analysis method for asymmetric resonator transmission applied to superconducting devices," *J. Appl. Phys.*, vol. 111, no. 5, Mar. 2012, Art. no. 054510.

[21] G. Nikandish, R. B. Staszewski, and A. Zhu, "Breaking the bandwidth limit: A review of broadband Doherty power amplifier design for 5G," *IEEE Microw. Mag.*, vol. 21, no. 4, pp. 57–75, Apr. 2020.

[22] C. Florian, P. A. Traverso, and A. Santarelli, "A Ka-band MMIC LNA in GaN-on-Si 100-nm technology for high dynamic range radar receivers," *IEEE Microw. Wireless Compon. Lett.*, vol. 31, no. 2, pp. 161–164, Feb. 2021.

[23] W. Liu et al., "6.2 W/mm and record 33.8% PAE at 94 GHz from N-polar GaN deep recess MIS-HEMTs with ALD Ru gates," *IEEE Microw. Wireless Compon. Lett.*, vol. 31, no. 6, pp. 748–751, Jun. 2021.

[24] A. Piacibello et al., "A 5-W GaN Doherty amplifier for Ka-band satellite downlink with 4-GHz bandwidth and 17-dB NPR," *IEEE Microw. Wireless Compon. Lett.*, vol. 32, no. 8, pp. 964–967, Aug. 2022.

[25] J.-S. Moon et al., "W-band graded-channel GaN HEMTs with record 45% power-added-efficiency at 94 GHz," *IEEE Microw. Wireless Technol. Lett.*, vol. 33, no. 2, pp. 161–164, Feb. 2023.

[26] N. Pompeo, K. Torokhtii, F. Leccese, A. Scorza, S. Sciuto, and E. Silva, "Fitting strategy of resonance curves from microwave resonators with non-idealities," in *Proc. IEEE Int. Instrum. Meas. Technol. Conf. (I2MTC)*, Turin, Italy, May 2017, pp. 1–6.

[27] G. Gugliandolo et al., "A split-ring resonator with interdigitated electrodes aimed at the dielectric characterization of liquid mixtures (invited paper)," in *Proc. IEEE Int. Conf. Integr. Circuits, Technol. Appl. (ICTA)*, Xi'an, China, Oct. 2022, pp. 137–141.

[28] J. B. Mehl, "Analysis of resonance standing-wave measurements," *J. Acoust. Soc. Amer.*, vol. 64, no. 5, pp. 1523–1525, Nov. 1978.

[29] C. Ramella, S. Corbellini, M. Pirola, L. Yu, and V. C. Fernicola, "Investigations on instability effects in a sapphire-based whispering gallery mode thermometer," in *Proc. IEEE Int. Instrum. Meas. Technol. Conf. (I2MTC)*, Turin, Italy, May 2017, pp. 1–6.

[30] G. Gugliandolo, S. Tabandeh, L. Rosso, D. Smorgon, and V. Fernicola, "Whispering gallery mode resonators for precision temperature metrology applications," *Sensors*, vol. 21, no. 8, p. 2844, Apr. 2021.

[31] W. C. Navidi, *Statistics for Engineers and Scientists*. New York, NY, USA: McGraw-Hill, 2006.

[32] G. Crupi, A. Raffo, G. Avolio, D. M. M.-P. Schreurs, G. Vannini, and A. Caddemi, "Temperature influence on GaN HEMT equivalent circuit," *IEEE Microw. Wireless Compon. Lett.*, vol. 26, no. 10, pp. 813–815, Oct. 2016.

Open Access funding provided by 'Università degli Studi di Messina' within the CRUI CARE Agreement